Unveiling different structural orderings in $Fe_{5-x}GeTe_2$

Vaibhav Walve,[1] Piyush Parakh,[1] Umashankar Rajput,[1] Akash S. Mhase,[2] Kirandeep Singh,[2] and Aparna Deshpande[1]
[1]*Department of Physics, Indian Institute of Science Education and Research Pune, Pune 411008, India*
[2]*Physical and Material Chemistry Division, CSIR - National Chemical Laboratory (CSIR-NCL), Pune 411008, India*

(Received 8 April 2024; revised 26 June 2024; accepted 25 July 2024; published 9 August 2024)

We investigate the metallic van der Waals itinerant ferromagnet $Fe_{5-x}GeTe_2$ with atomic scale, spatially resolved low-temperature scanning tunneling microscopy (STM), and spectroscopy (STS). STM images unveil a new structural order $2a \times 1a$ along with the known order $\sqrt{3}a \times \sqrt{3}a$ manifesting as nonuniform domains. STS shows spatial and energy resolved local density of states that reveal the crucial influence of Fe(1) site occupancy on the system's electronic interactions. Our magnetization measurements show magnetic anomalies at lower temperatures and identify a Curie temperature (T_c) surpassing room temperature. Collectively, our results elucidate the intricate nature of $Fe_{5-x}GeTe_2$ and underscore its potential for tunability of spintronics and high-temperature magnetic applications.

DOI: 10.1103/PhysRevB.110.075119

I. INTRODUCTION

Magnetic van der Waals (M-vdW) materials offer the possibility to study magnetism in two dimensions (2D), as individual monolayers, bilayers, or as heterostructures with other vdW materials. Coupled with this comes the essential aspect of tuning these materials for various applications. M-vdWs can be ferromagnetic and antiferromagnetic, and within these two broad classes, depending on the band structure, M-vdWs are semiconducting, insulating, or metallic [1].

In the case of metallic ferromagnets, the mutual effect of spin and charge leads to itinerant as well as localized phenomena. The interplay between exchange interactions originating due to spin, and electronic correlations owing to the charges in metals, continues to be an exciting question. While exchange interactions favor magnetism, electronic correlations manifest as charge density waves [2,3]. The notion of correlations among itinerant electrons, coupled with the exchange interactions, was initially proposed by Wigner [4]. For itinerant ferromagnets, a preference for nonlocal strong electronic correlations is established through band renormalization [5]. These strong correlations manifest as intriguing electronic phenomena, including ferromagnetic superconductivity, charge ordering, and nontrivial topology [6,7].

The family of compounds Fe_nGeTe_2 where $3 \leqslant n \leqslant 7$ shows the coexistence of itinerant and localized magnetism [8]. Bulk Fe_3GeTe_2 has gathered significant attention due to its room-temperature ferromagnetism under ionic gating conditions [9]. Large Berry curvature observed at the Fermi level gives rise to prominent anomalous Hall effect, and the topological spin texture remains stable at higher temperatures [10–12]. *Ab initio* calculations employing density functional theory (DFT) indicate the potential for achieving higher stable structures in Fe_nGeTe_2 by increasing the Fe content, where $n \geqslant 3$ [13]. Fe doping is recognized to enhance the ordering temperature beyond room temperature and theoretically stable structures are predicted up to $n = 6$, establishing a limit for increasing the transition temperature (T_c) through Fe addition [13,14]. The bulk Fe_5GeTe_2 shows ferromagnetic order at room temperature ($T_c = 310$ K) [15].

The $Fe_{5-x}GeTe_2$ system is interesting, as the structural reconstructions affect its electronic and magnetic properties. Experimental reports on $Fe_{5-x}GeTe_2$ have shown a structural reconstruction of $\sqrt{3}a \times \sqrt{3}a$ [16,17]. Some studies attribute it to a checkerboard arrangement of Fe ions beneath the Te layers that is energetically favorable, or the breaking of Fe(1)-Ge inversion symmetry [18,19]. One more intriguing aspect is the increase in T_c. The anomalous transition in magnetization occurs at lower temperatures resulting in an increase in the anisotropy along the easy axis [13,15]. Despite the observed increase in T_c, experimental results suggest the possible origin to be either antiferromagnetic coupling or the emergence of ferrimagnetic domains in the structure, causing a decrease in magnetization at lower temperatures [18,20,21].

Is this $\sqrt{3}a \times \sqrt{3}a$ reconstruction unique? Can there be competing phases at similar energies? Is there a variation in T_c? To address these aspects we study the single crystal $Fe_{5-x}GeTe_2$. We probe the local dynamics of the itinerant electrons and their spatial fingerprints with atomically and spatially resolved STM and STS measurements at 4.2 K. We confirm the sample stoichiometry through TEM elemental analysis. Our STM images show the $2a \times 1a$ reconstruction along with the $\sqrt{3}a \times \sqrt{3}a$ order. We also perform global magnetization measurements to gain insight into the magnetic nature of the $Fe_{5-x}GeTe_2$ single crystal. Our results indicate that structural reconstruction leads to site-dependent hybridizations and modified interactions among itinerant electrons. The heavy ligand coupling with different Fe sites presumably causes the anomalous behavior observed at lower temperatures.

II. METHODS

Single crystal $Fe_{5-x}GeTe_2$ purchased from 2D semiconductors was used for this study [22]. A crystal piece was suspended in acetone and subjected to sonication for one

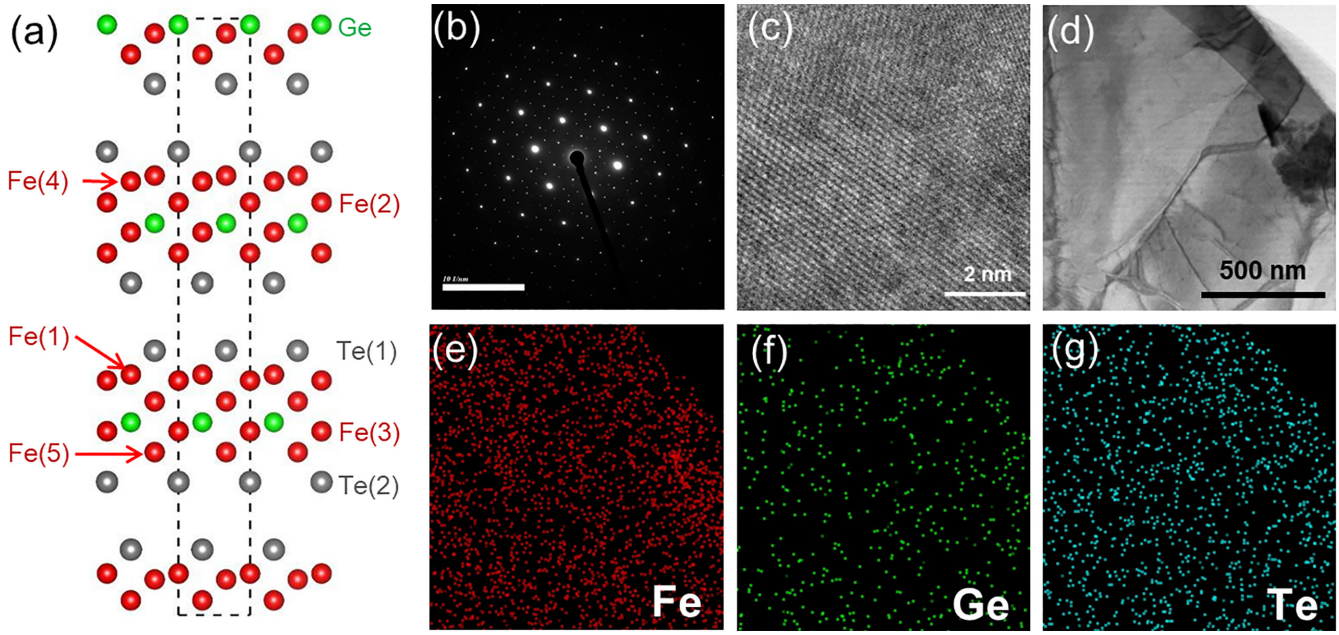

FIG. 1. (a) Crystal structure of $Fe_{5-x}GeTe_2$ showing the side view of unit cell (dotted rectangle marks the unit cell). The different sites of Fe, Ge, and Te atoms are shown in the structure. (b) SAED pattern collected over the $Fe_{5-x}GeTe_2$ flake (c) HR-TEM image corresponding to (b) showing the arrangement of Te atoms in the layer. (d) HR-TEM image of $Fe_{5-x}GeTe_2$ flake. The elemental mapping of Fe, Ge, and Te over the $Fe_{5-x}GeTe_2$ flake is shown in (e)–(g), respectively.

hour to achieve thinner flakes suitable for high-resolution transmission electron microscope (HR-TEM) imaging. Characterization of the $Fe_{5-x}GeTe_2$ crystal was performed using the HR-TEM Joel JEM2200FS model. This HR-TEM has a Gatan camera and an Oxford Systems x-ray detector. The imaging process was performed at a beam energy of 200 keV, while elemental analysis was conducted at a beam energy of 20 keV. Structural characterization was ensured by analyzing selected area electron diffraction (SAED) patterns and elemental mapping across multiple crystals to confirm the structural composition of $Fe_{5-x}GeTe_2$. Many such flakes were imaged using HR-TEM.

For STM measurements a crystal piece with dimensions of 2 mm × 2 mm was affixed to the sample plate using silver epoxy. The silver epoxy was then allowed to cure at a temperature of 150 °C in a vacuum furnace, maintained at a pressure of $\sim 10^{-6}$ mbar to prevent crystal oxidation. The sample was then transferred to the ultra high vacuum (UHV) sample preparation chamber for *in situ* exfoliation. The top layer of the $Fe_{5-x}GeTe_2$ crystal was exfoliated using Scotch^{TM}tape to obtain a clean and fresh surface prior to immediate transfer to the STM chamber for measurements. STM measurements were conducted using the Scienta Omicron low-temperature ultrahigh vacuum scanning tunneling microscope (LT-UHV-STM) at a base temperature of 4.3 K and a base pressure of 2×10^{-9} mbar. An electrochemically etched tungsten tip was used for imaging. Several trials of imaging and spectroscopy were carried out with different tips. The images were processed using the image analysis software (SPIP 6.0.9, Image Metrology, Denmark). The local density of states (LDOS) was determined by STS. Using the standard lock-in technique, a modulation voltage of 6 mV at 652 Hz frequency was applied with the SRS lock-in amplifier. The tunneling voltage (V) was varied within 200 mV, and the corresponding variation in the current (I) was obtained as a dI/dV spectrum, thus giving the tunneling conductance for $Fe_{5-x}GeTe_2$.

For magnetic properties measurement, Quantum Design (QD) magnetic property measurement system (MPMS) was used. The $Fe_{5-x}GeTe_2$ single crystal was placed parallel to the applied field ($H_{applied} \parallel ab$ plane). Magnetization measurements were conducted in both zero-field-cooled (ZFC) and field-cooled (FC) modes at 1000 Oe with the temperature varying from 300 K to 5 K. Additionally, magnetization was measured at 5 K and 300 K under varying magnetic fields up to 60 kOe.

III. RESULTS AND DISCUSSION

$Fe_{5-x}GeTe_2$ crystallizes in a rhombohedral lattice symmetry with the centrosymmetric space group $R\bar{3}m$ [15,23,24]. Figure 1(a) illustrates the crystal structure of $Fe_{5-x}GeTe_2$, highlighting the distinct site occupancies of Fe, Ge, and Te atoms within the structure. Notably, the Fe(1) site exhibits partial occupancy, leading to a split-site configuration for the Ge atoms. Using HR-TEM measurements, the crystalline nature and stoichiometry were determined. Intense and sharp peaks in the SAED pattern [as shown in Fig. 1(b)] confirmed the crystalline nature of the sample. The Te atomic arrangement is displayed in the corresponding high resolution image, Fig. 1(c). The stoichiometry of our sample was confirmed through HR-TEM elemental analysis, which was performed on different flakes of the crystal, revealing slight variations in the atomic concentration among them. The stoichiometry of this crystal was determined to be $\sim Fe_{4.8}GeTe_2$. In Fig. 1(d), a typical flake is illustrated, and its elemental mapping of Fe, Ge, and Te elements are shown in Figs. 1(e)–1(g), respectively.

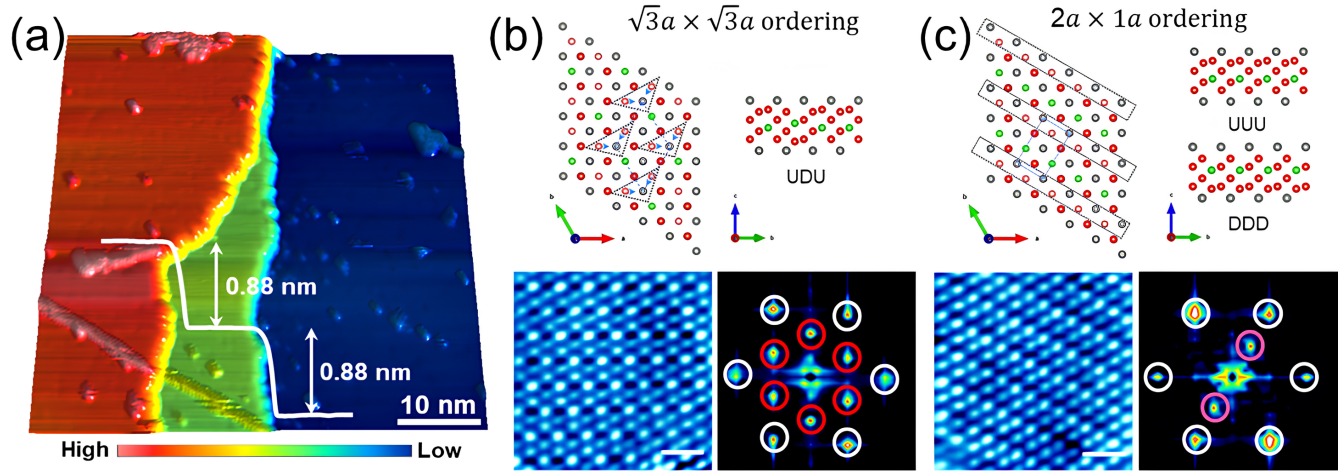

FIG. 2. (a) 3D view of the $Fe_{5-x}GeTe_2$ surface (V = 1 V, I = 0.1 nA) showing layer cascade. The layer height profile is shown with the white trace, the single-layer height is measured to be 0.88 nm. (b) In the upper panel, the structural origin of the UDU arrangement is shown in the top view (left) and side view (right). The STM topographic image shown in lower left is $\sqrt{3}a \times \sqrt{3}aR30^\circ$ structural ordering (V = −100 mV, I = 100 pA). To the lower right is the corresponding FFT of the STM image, which shows the lattice peak (marked by white circles) and the structural ordering peaks (marked by red circles). (c) In the upper panel, the top view (left) and side view (right) of the structural arrangement with alternating UUU and DDD stripes is shown. The STM topographic image shown in lower left is $2a \times 1a$ structural ordering (V = −100 mV, I = 100 pA). The lower right shows the corresponding FFT of the STM image, which shows the lattice peaks (marked in white) and the structural ordering peaks (marked in magenta).

Figure 2(a) is a large area STM image that shows the $Fe_{5-x}GeTe_2$ layer cascade. Our step height measurement yields the height to be 0.88 nm. Which is higher than the layer thickness of 0.82 nm in Fe_3GeTe_2 [25]. This could be understood by the structural difference among them.

In our study, we have identified two distinct types of structural ordering in the $Fe_{5-x}GeTe_2$ sample. These are revealed in the topography images of the regions examined. The first type of ordering, $\sqrt{3}a \times \sqrt{3}a$, is shown in Fig. 2(b). The second type of ordering, $2a \times 1a$, is shown in Fig. 2(c). The measured lattice spacing is 0.4 nm through the line profile of actual STM images, which was further validated by k-space fast Fourier transform (FFT) analysis for both regions. Within the limits of our experimental resolution, no significant changes in lattice parameters were observed.

The $\sqrt{3}a \times \sqrt{3}a$ arrangement has been frequently observed in prior STM and XRD results [15–17]. The detailed structural theory is proposed by Ershad *et al.* [19]. According to the theory, depending on the Fe(1) site occupancy, there are two types of structural ordering: UDU and UUU/DDD. In this context, "U" indicates a Fe(1) atom located near the upper Te surface of the layer, while "D" signifies a Fe(1) atom positioned near the lower Te surface of the layer. The UDU ordering describes a sequence where Fe(1) occupies alternating positions of "U" and "D." The UUU/DDD ordering is characterized by Fe(1) exclusively occupying "UUU/DDD" positions. Among these, UDU ordering is generally preferred due to its lower formation energy, whereas UUU/DDD ordering, possessing a higher formation energy, is more elusive in $Fe_{5-x}GeTe_2$ [19].

However, we observed the striped structural ordering $2a \times 1a$, as depicted in Fig. 2(c). This pattern, unlike the $\sqrt{3}a \times \sqrt{3}a$, is the new finding of our work. It can be explained by an alternating line sequence of UUU and DDD, which creates stripes across the surface. The corresponding striped pattern is observed in the STM topography image [lower left of Fig. 2(c)]. The FFT of the area clearly exhibits inner peaks corresponding to the $2a \times 1a$ structure [lower right of Fig. 2(c)].

In our STM images, $\sqrt{3}a \times \sqrt{3}a$ modulations are seen over most of the regions, as previously observed in $Fe_{5-x}GeTe_2$ [16,17]. The upper right region of Fig. 3(a), outlined by red dashed lines, prominently displays a $\sqrt{3}a \times \sqrt{3}a$ ordering. The lower left region marked with cyan dashed lines exhibits striped features with a $2a \times 1a$ ordering. Both these modulations coexist in the same region. The background corrugation over the surface can be seen as the local strain over the surface, which could be due to the Fe intercalation that is common in $Fe_{5-x}GeTe_2$ [27,28]. The surface corrugation exhibits no periodicity, thereby ruling out moirlike behavior. Previous studies on van der Waals materials have suggested that intercalation between the layers leads to corrugation formation over the surface [29,30].

To differentiate between the two observed phases $\sqrt{3}a \times \sqrt{3}a$ and $2a \times 1a$ in Fig. 3(a), we measured dI/dV maps to get a spatial variation of the local density of states (LDOS) on the structurally ordered regions. These maps are shown in Figs. 3(b)–3(f). With spectroscopic imaging, we effectively distinguish between two regions at the different energies from 1 mV (close to Fermi energy), 76.63 mV, 125 mV, 174.02 mV, and 250 mV in the conduction band. We have not observed any significant changes in the valence band; hence, corresponding energies are not included. The color scale indicates the relative value of LDOS. At 1 mV bias [Fig. 3(b)], close to the Fermi energy, we observe a lower LDOS at the Fermi energy for the $2a \times 1a$ region compared to the $\sqrt{3}a \times \sqrt{3}a$ region. As we move away from the Fermi energy in the conduction band, the LDOS difference between the regions diminishes, as depicted at 76.63 mV bias [Fig. 3(c)]. No distinguishable features are found at an energy of 125 meV

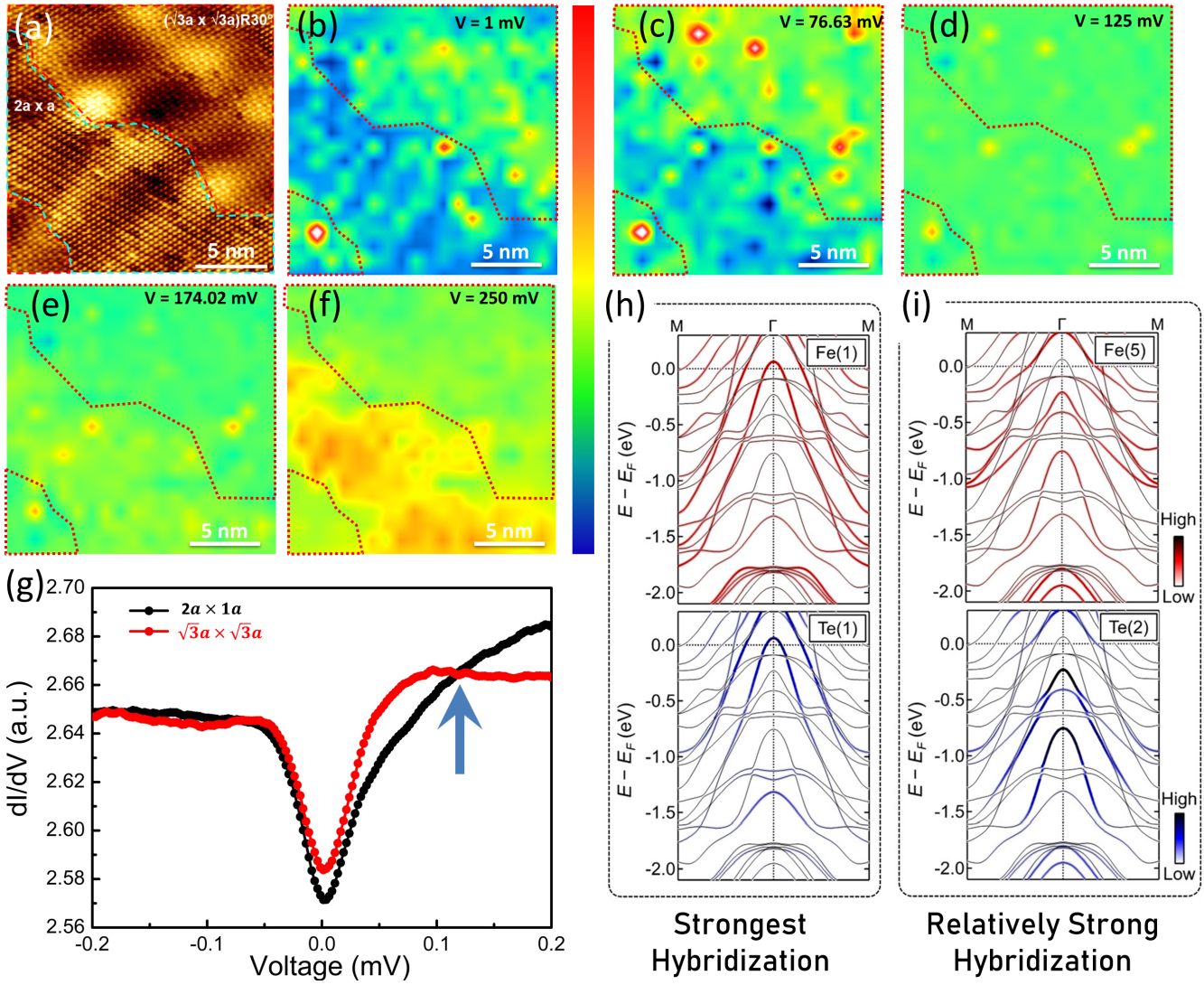

FIG. 3. (a) STM image with $(\sqrt{3}a \times \sqrt{3}a)R30^\circ$ highlighted in red and $(2a \times 1a)$ region highlighted in cyan (V = −100 mV, I = 0.1 nA). (b)–(f) dI/dV maps taken over regions shown in (a) at a bias voltage of (b) V = 1 mV, (c) 76.63 mV, (d) V = 125 mV, (e) V = 174.02 mV, and (f) 250 mV. (g) dI/dV spectroscopy over the $\sqrt{3}a \times \sqrt{3}a$ and $2a \times 1a$ regions, with the crossover of the LDOS between both regions marked in blue near 125 meV. (h), (i) The DFT + GGA calculated band structure illustrates the relative spectral weight for hybridized Fe d orbitals and Te p orbitals for different site occupancy. Red denotes d orbital dominance, while blue represents p orbital dominance. Panel (h) shows the strongest hybridization between Fe(1) and Te(1), whereas panel (i) exhibits relatively strong hybridization between Fe(5) and Te(2) sites (adopted from Ref. [26]).

[Fig. 3(d)], indicating a crossover point where nearly the same LDOS is observed for both regions. This is reflected in the uniform color of the LDOS map. Beyond 125 meV, the LDOS is observed to be higher for the $2a \times 1a$ region than the $\sqrt{3}a \times \sqrt{3}a$ region, as seen at 174.02 mV [Fig. 3(e)]. At 250 meV [Fig. 3(f)], a complete inversion of LDOS is observed over the regions compared to the Fermi energy.

We performed comparative dI/dV point spectroscopy over both regions, as shown in Fig. 3(g). There is no significant change in the LDOS in the valence band as seen in the overlap of red and black spectra. However, at the Fermi energy, we observe a dip in the LDOS, possibly arising from the strong hybridization between the magnetic Fe atoms and nonmagnetic Te atoms [26]. Interestingly, the dip observed for the $2a \times 1a$ region (black curve) is more pronounced than for the $\sqrt{3}a \times \sqrt{3}a$ region (red curve). A crossover in the LDOS is evident at a bias voltage near 125 mV (marked with a blue arrow). Beyond 125 mV, we observe a higher LDOS for the $2a \times 1a$ region compared to the $\sqrt{3}a \times \sqrt{3}a$ region, consistent with the trend in the LDOS maps over both regions. This experimental confirmation can be further compared with theoretical calculations by Yamagami *et al.* [26].

In the determination of the physical properties of $Fe_{5-x}GeTe_2$, the Fe(1) atomic site plays a crucial role. Understanding the site-dependent role in the observed LDOS over both regions is imperative. Figures 3(h) and 3(i) present DFT+GGA calculations (adopted from the supporting online material of [26]) for different Fe and Te sites, showing their hybridization in Fe $3d$ orbitals and Te $5p$ orbitals near the Fermi energy. To simplify the DFT calculations, Fe(1) occupancy is assumed to be 100% and not random. The $5p$ delocalized orbitals of Te and $3d$ localized orbitals of Fe

exhibit antiparallel spin polarization, evident from the relative spectral weight of the band structure. The strongest hybridization is observed between Fe(1) and Te(1) sites, with higher spectral weight near the Fermi energy. A relatively stronger hybridization is observed between Fe(5) and Te(2) sites, with higher spectral weight around 250 meV. These results can be compared with the LDOS experiment for both regions. The $\sqrt{3}a \times \sqrt{3}a$ region shows nearly the same LDOS for the conduction band, suggesting equivalent contributions from Fe(1) and Fe(5) sites. The symmetric isotropic structural arrangement could be the reason for this. In contrast, for the $2a \times 1a$ region, Fe(1) contributes less sites than Fe(5) to LDOS, highlighting the important role of structural ordering in energy level hybridization. Thus, our LDOS maps provide direct evidence for the predicted spectral weights of the band structure reported in Ref. [26].

The simple Stoner model cannot be used to explain the itinerant magnetism in $Fe_{5-x}GeTe_2$. The magnetism in the $Fe_{5-x}GeTe_2$ sample can be explained by a combination of itinerant and localized moments. Fe $3d$ orbitals are localized in nature, while Te $5p$ orbitals have delocalized itinerant electrons. Yamagami *et al.* predicted that strongly hybridizing localized Fe spins with the delocalized nonmagnetic Te ligands is crucial in determining the higher T_c in $Fe_{5-x}GeTe_2$ [26]. Strong hybridization with the Fe $3d$ bands induces spin polarization in the Te/Ge ligands band, but they align antiparallel to the Fe spin-polarized bands. The spin-polarized density of states (SP-DOS) of the ligands is expected to be higher for hybridized bands located near the Fermi energy, directly affecting the T_c. The closer the hybridized band to the Fermi energy, the higher the T_c. This indicates that the $\sqrt{3}a \times \sqrt{3}a$ ordering has a higher T_c compared to the $2a \times 1a$ ordering, as it possesses the strongest hybridized band near the Fermi energy and has a higher LDOS. The spin polarization of the Te/Ge ligands by Fe spins introduces strong spin-orbit coupling, causing the magnetoanisotropic effect observed previously in the FePt intermetallic system [31,32]. This magnetoanisotropic effect plays an important role in the observed magnetic anomalies.

To highlight the role of the magnetoanisotropic effect in $Fe_{5-x}GeTe_2$, we performed magnetization measurements. In Fig. 4(a), we present zero-field cooled (ZFC) and field-cooled (FC) magnetization data at an applied magnetic field of 1000 Oe. The presented data closely matches with $Fe_{5-x}GeTe_2$ [13,15]. A notable upturn (shown by the green arrow) in the magnetic data near 280 K could be misunderstood as the Curie temperature T_c. The exact measurement of T_c could be confirmed by M-H measurements. The M-H measurements, Fig. 4(b), are taken at 300 K (black) and 5 K (red). Above T_c, we expect a linear M-H relationship, as observed in a paramagnetic sample. The M-H measurements reveal a well-saturated S-shaped magnetic hysteresis loop at 300 K, affirming that the T_c for our $Fe_{5-x}GeTe_2$ samples exceeds room temperature. This is further supported by a nonzero magnetic moment, as is evident in the M-T data.

A broad cusp observed in the temperature range of 110 K to 280 K can be attributed to simple anisotropy changes in $Fe_{5-x}GeTe_2$ [13,15]. Within this range, there is a negligible shift in ZFC and FC magnetization, consistent with initial

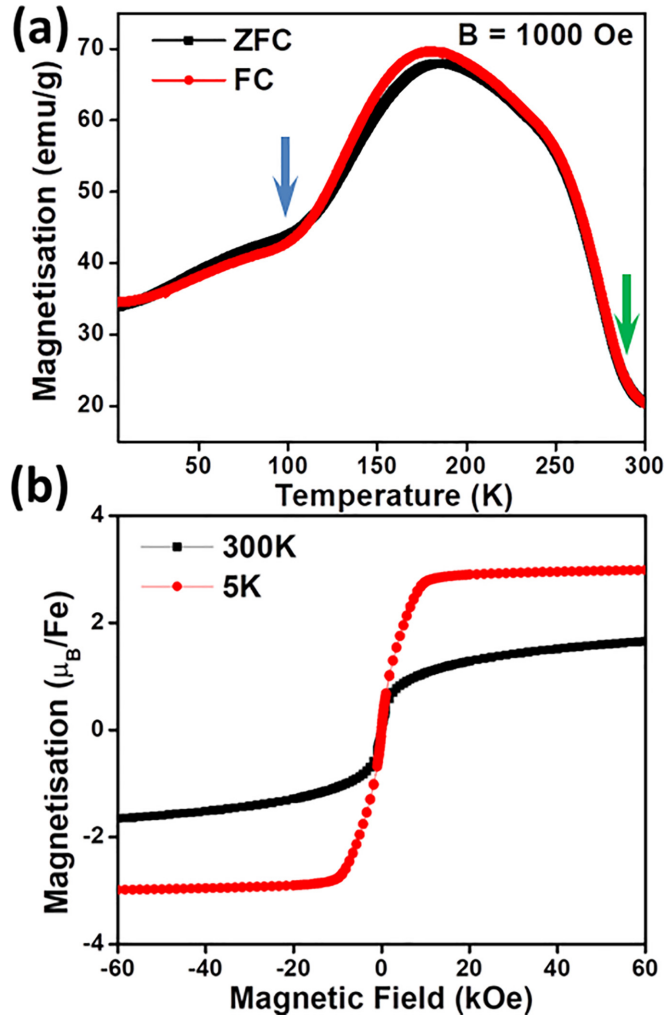

FIG. 4. (a) Temperature dependent magnetization on the $Fe_{5-x}GeTe_2$ crystal where the black plot shows zero field cooled (ZFC) magnetization and the red plot shows field cooled (FC) magnetization. (b) M-H measurements taken at 5 K and 300 K.

reports that observed no thermal hysteresis along the *ab* plane [20]. In this region, ferromagnetic ordering explains the magnetism, while an anisotropy changes spin-spin interactions [13,15].

At the transition temperature of 110 K (shown by the blue arrow), magnetic anomalies emerge, a phenomenon observed by many researchers for $Fe_{5-x}GeTe_2$ single crystals [13,16,17]. The decrease in magnetization along the *ab* plane suggests a rotation of the easy axis from the *ab* plane to the *c* axis in the sample [13]. These anomalies align with the effect of strong spin-orbit coupling with the Ge/Te ligands assisted with anomalous structural expansion noted in neutron diffraction, indicating magnetoelastic coupling in the structure [15,26]. The decline in magnetization suggests the presence of antiferromagnetic (AFM) interactions within the structure, likely due to the Fe(1) site occupancy and antiparallel coupling with the ligands. These AFM interactions are likely localized within specific regions, giving rise to bubblelike domains [21]. This localized behavior aligns with the overall

restoration of ferromagnetic properties, as illustrated in the M-H data at 5 K in Fig. 4(b).

Thus, the strongest hybridization between Te/Ge ligands and the Fe(1) site is crucial for T_c, and its antiparallel coupling influences the magnetic properties. The strongly hybridized local density of states (LDOS) near the Fermi energy in $\sqrt{3}a \times \sqrt{3}a$ ordering is more prominent than the $2a \times 1a$ ordering, which could be attributed to higher T_c for $\sqrt{3}a \times \sqrt{3}a$ ordering. This suggests that the $\sqrt{3}a \times \sqrt{3}a$ reconstruction observed in many STM and XRD studies plays an important role observed higher T_c in $Fe_{5-x}GeTe_2$ [16–18]. It also reduces magnetization at lower temperatures due to the antiparallel coupling of Te ligands and Fe(1) in $Fe_{5-x}GeTe_2$ [26].

Similar observations in the MnBi system have noted that changes in Mn occupancy within different sites influence spin-spin correlations in ferromagnets [33]. Below 110 K, structural transformations appear to drive the moment of Fe ions at interstitial sites, altering spin-spin correlations among Fe ions coupling and giving rise to antiferromagnetic (AFM) bubblelike domains, as observed in various experiments [14,21]. Additionally, strong spin-orbit coupling, originating from spin-polarized bands of ligands, changes magnetic anisotropy and may cause the rotation of the easy axis, as reported previously [34]. The inception of AFM domains and easy axis rotation due to strong spin-orbit coupling contributes to a reduction in magnetization, a phenomenon evident in our magnetic results.

IV. CONCLUSION

In our investigation of the van der Waals metallic magnet $Fe_{5-x}GeTe_2$, we conducted comprehensive local STM and STS measurements, along with global magnetization measurements. We observe a structural ordering of $2a \times 1a$ in addition to the previously reported $\sqrt{3}a \times \sqrt{3}a$ ordering. The $\sqrt{3}a \times \sqrt{3}a$ ordering plays an important role in the higher T_c observed for $Fe_{5-x}GeTe_2$. The Fe(1) site occupancy and strong hybridization of the nonmagnetic ligands are crucial in determining the magnetic properties of $Fe_{5-x}GeTe_2$. Our magnetization measurements confirm that the Curie temperature exceeds room temperature, consistent with previous reports for $Fe_{5-x}GeTe_2$. Anomalies in magnetization at lower temperatures are associated with AFM interactions involving heavy ligands and the Fe(1) site, as well as strong spin-orbit coupling. Our study establishes a connection between these magnetization anomalies and the strong hybridization of heavy ligands and Fe(1) ions in this system. This sets the stage for comprehensive theoretical investigations to pin down the exact mechanisms underlying these phenomena.

ACKNOWLEDGMENTS

We are grateful to the Indian Institute of Science Education and Research (IISER), Pune, for their financial assistance and instrumental facilities. V.W. acknowledges the financial support provided by the CSIR, Government of India, in the form of a Research Fellowship. U.R. acknowledges the financial assistance received from UGC India in the form of a research fellowship. A.S.M. is thankful to CSIR-NCL Central Analytical Facility (CAF) for financial support in terms of the fellowship. K.S. is grateful to DST-SERB, Government of India, for the project funded under EMEQ scheme-2022 (EEQ/2021/000242).

[1] K. S. Burch, D. Mandrus, and J.-G. Park, Magnetism in two-dimensional van der Waals materials, Nature (London) **563**, 47 (2018).

[2] C.-W. Chen, J. Choe, and E. Morosan, Charge density waves in strongly correlated electron systems, Rep. Prog. Phys. **79**, 084505 (2016).

[3] A. F. Fang, X. B. Wang, P. Zheng, and N. L. Wang, Unconventional charge-density wave in $Sr_3Ir_4Sn_{13}$ cubic superconductor revealed by optical spectroscopy study, Phys. Rev. B **90**, 035115 (2014).

[4] E. Wigner, On the interaction of electrons in metals, Phys. Rev. **46**, 1002 (1934).

[5] C. Tusche, M. Ellguth, V. Feyer, A. Krasyuk, C. Wiemann, J. Henk, C. M. Schneider, and J. Kirschner, Nonlocal electron correlations in an itinerant ferromagnet, Nat. Commun. **9**, 3727 (2018).

[6] N. Maksimovic, R. Day, A. Liebman-Peláez, F. Wan, N.-H. Jo, C. Jozwiak, A. Bostwick, E. Rotenberg, S. Griffin, J. Singleton *et al.*, Strongly correlated itinerant magnetism near superconductivity in $NiTa_4Se_8$, Phys. Rev. B **106**, 224429 (2022).

[7] S. Shao, J.-X. Yin, I. Belopolski, J.-Y. You, T. Hou, H. Chen, Y. Jiang, M. S. Hossain, M. Yahyavi, C.-H. Hsu *et al.*, Intertwining of magnetism and charge ordering in kagome FeGe, ACS Nano **17**, 10164 (2023).

[8] J.-X. Zhu, M. Janoschek, D. S. Chaves, J. C. Cezar, T. Durakiewicz, F. Ronning, Y. Sassa, M. Mansson, B. L. Scott, N. Wakeham *et al.*, Electronic correlation and magnetism in the ferromagnetic metal Fe_3GeTe_2, Phys. Rev. B **93**, 144404 (2016).

[9] Y. Deng, Y. Yu, Y. Song, J. Zhang, N. Z. Wang, Z. Sun, Y. Yi, Y. Z. Wu, S. Wu, J. Zhu *et al.*, Gate-tunable room-temperature ferromagnetism in two-dimensional Fe_3GeTe_2, Nature (London) **563**, 94 (2018).

[10] K. Kim, J. Seo, E. Lee, K.-T. Ko, B. Kim, B. G. Jang, J. M. Ok, J. Lee, Y. J. Jo, W. Kang *et al.*, Large anomalous Hall current induced by topological nodal lines in a ferromagnetic van der Waals semimetal, Nat. Mater. **17**, 794 (2018).

[11] J. Xu, W. A. Phelan, and C.-L. Chien, Large anomalous Nernst effect in a van der Waals ferromagnet Fe_3GeTe_2, Nano Lett. **19**, 8250 (2019).

[12] B. Ding, Z. Li, G. Xu, H. Li, Z. Hou, E. Liu, X. Xi, F. Xu, Y. Yao, and W. Wang, Observation of magnetic skyrmion bubbles in a van der Waals ferromagnet Fe_3GeTe_2, Nano Lett. **20**, 868 (2020).

[13] J. Seo, D. Y. Kim, E. S. An, K. Kim, G.-Y. Kim, S.-Y. Hwang, D. W. Kim, B. G. Jang, H. Kim, G. Eom *et al.*, Nearly room temperature ferromagnetism in a magnetic metal-rich van der Waals metal, Sci. Adv. **6**, eaay8912 (2020).

[14] S. Liu, Z. Li, K. Yang, E. Zhang, A. Narayan, X. Zhang, J. Zhu, W. Liu, Z. Liao, M. Kudo *et al.*, Tuning 2D magnetism in $Fe_{3+x}GeTe_2$ films by element doping, Natl. Sci. Rev. **9**, nwab117 (2022).

[15] A. F. May, D. Ovchinnikov, Q. Zheng, R. Hermann, S. Calder, B. Huang, Z. Fei, Y. Liu, X. Xu, and M. A. McGuire, Ferromagnetism near room temperature in the cleavable van der Waals crystal Fe_5GeTe_2, ACS Nano **13**, 4436 (2019).

[16] T. T. Ly, J. Park, K. Kim, H.-B. Ahn, N. J. Lee, K. Kim, T.-E. Park, G. Duvjir, N. H. Lam, K. Jang *et al.*, Direct observation of Fe-Ge ordering in $Fe_{5-x}GeTe_2$ crystals and resultant helimagnetism, Adv. Funct. Mater. **31**, 2009758 (2021).

[17] X. Wu, L. Lei, Q. Yin, N.-N. Zhao, M. Li, Z. Wang, Q. Liu, W. Song, H. Ma, P. Ding *et al.*, Direct observation of competition between charge order and itinerant ferromagnetism in the van der Waals crystal $Fe_{5-x}GeTe_2$, Phys. Rev. B **104**, 165101 (2021).

[18] A. F. May, M.-H. Du, V. R. Cooper, and M. A. McGuire, Tuning magnetic order in the van der Waals metal Fe_5GeTe_2 by cobalt substitution, Phys. Rev. Mater. **4**, 074008 (2020).

[19] S. Ershadrad, S. Ghosh, D. Wang, Y. Kvashnin, and B. Sanyal, Unusual magnetic features in two-dimensional Fe_5GeTe_2 induced by structural reconstructions, J. Phys. Chem. Lett. **13**, 4877 (2022).

[20] C.-K. Tian, C. Wang, W. Ji, J.-C. Wang, T.-L. Xia, L. Wang, J.-J. Liu, H.-X. Zhang, and P. Cheng, Domain wall pinning and hard magnetic phase in co-doped bulk single crystalline Fe_3GeTe_2, Phys. Rev. B **99**, 184428 (2019).

[21] J. Yi, H. Zhuang, Q. Zou, Z. Wu, G. Cao, S. Tang, S. Calder, P. Kent, D. Mandrus, and Z. Gai, Competing antiferromagnetism in a quasi-2D itinerant ferromagnet: Fe_3GeTe_2, 2D Mater. **4**, 011005 (2016).

[22] 2d semiconductors, https://www.2dsemiconductors.com/.

[23] Z. Li, W. Xia, H. Su, Z. Yu, Y. Fu, L. Chen, X. Wang, N. Yu, Z. Zou, and Y. Guo, Magnetic critical behavior of the van der Waals Fe_5GeTe_2 crystal with near room temperature ferromagnetism, Sci. Rep. **10**, 15345 (2020).

[24] M. Schmitt, T. Denneulin, A. Kovács, T. G. Saunderson, P. Rüßmann, A. Shahee, T. Scholz, A. H. Tavabi, M. Gradhand, P. Mavropoulos *et al.*, Skyrmionic spin structures in layered Fe_5GeTe_2 up to room temperature, Commun. Phys. **5**, 254 (2022).

[25] M. Zhao, B.-B. Chen, Y. Xi, Y. Zhao, H. Xu, H. Zhang, N. Cheng, H. Feng, J. Zhuang, F. Pan *et al.*, Kondo holes in the two-dimensional itinerant Ising ferromagnet Fe_3GeTe_2, Nano Lett. **21**, 6117 (2021).

[26] K. Yamagami, Y. Fujisawa, B. Driesen, C.-H. Hsu, K. Kawaguchi, H. Tanaka, T. Kondo, Y. Zhang, H. Wadati, K. Araki *et al.*, Itinerant ferromagnetism mediated by giant spin polarization of the metallic ligand band in the van der Waals magnet Fe_5GeTe_2, Phys. Rev. B **103**, L060403 (2021).

[27] M. Silinskas, S. Senz, P. Gargiani, B. Kalkofen, I. Kostanovskiy, K. Mohseni, H. L. Meyerheim, S. S. P. Parkin, and A. Bedoya-Pinto, Self-intercalation as origin of high-temperature ferromagnetism in epitaxially grown Fe_5GeTe_2 thin films, arXiv:2309.17439.

[28] H. Zhang, R. Chen, K. Zhai, X. Chen, L. Caretta, X. Huang, R. V. Chopdekar, J. Cao, J. Sun, J. Yao *et al.*, Itinerant ferromagnetism in van der Waals $Fe_{5-x}GeTe_2$ crystals above room temperature, Phys. Rev. B **102**, 064417 (2020).

[29] M. Hong, P. Yang, X. Zhou, S. Zhao, C. Xie, J. Shi, Z. Zhang, Q. Fu, and Y. Zhang, Decoupling the interaction between wet-transferred MoS_2 and graphite substrate by an interfacial water layer, Adv. Mater. Interfaces **5**, 1800641 (2018).

[30] S. Kovalenko, B. Andryushechkin, and K. Eltsov, STM study of oxygen intercalation at the graphene/Ni (111) interface, Carbon **164**, 198 (2020).

[31] I. V. Solovyev, P. H. Dederichs, and I. Mertig, Origin of orbital magnetization and magnetocrystalline anisotropy in *TX* ordered alloys (where T = Fe, Co and X = Pd, Pt), Phys. Rev. B **52**, 13419 (1995).

[32] K. Ikeda, T. Seki, G. Shibata, T. Kadono, K. Ishigami, Y. Takahashi, M. Horio, S. Sakamoto, Y. Nonaka, M. Sakamaki *et al.*, Magnetic anisotropy of $L1$-ordered FePt thin films studied by Fe and Pt $L_{2,3}$-edges x-ray magnetic circular dichroism, Appl. Phys. Lett. **111**, 142402 (2017).

[33] P. Kharel, R. Skomski, P. Lukashev, R. Sabirianov, and D. J. Sellmyer, Spin correlations and Kondo effect in a strong ferromagnet, Phys. Rev. B **84**, 014431 (2011).

[34] D. Dai, H. Xiang, and M.-H. Whangbo, Effects of spin-orbit coupling on magnetic properties of discrete and extended magnetic systems, J. Comput. Chem. **29**, 2187 (2008).